Believe It or Not: Incorporating Relative Time Delay and Magnification Distributions Predicted by Lens Models into Ranking Possible Sub-Threshold, Strongly-Lensed Candidates

Haley Boswell[a]

(Dated: July 9, 2023)

We expand upon gravitational-wave analysis by considering the possibility of gravitationally lensed pairs of gravitational waves, a phenomenon that has predominantly been studied in regard to electromagnetic waves. Much of the previously established research in gravitational lensing is extended to lensed gravitational waves due to similarity in behavior to electromagnetic waves. Under the lensing hypothesis, we assume the lensed counterparts are subthreshold due to the relative time delay between paths and consequential demagnification effects. The database of registered gravitational waves are considered potential super-threshold events, and the parameters of our search pipeline are altered so subthreshold events significant to the original waveform are registered as a trigger. We do this using the gstLAL-based TESLA search pipeline, which increases the likelihood of detecting these subthreshold events by optimizing the template bank and considering only templates capable of recovering the posterior samples given by Bayes probability distribution. The results are then ranked by the likelihood of the signal being astrophysical in origin and logged for further analysis to determine if they are a lensed counterpart. We aim to improve the TESLA method by modifying the search pipeline's code to produce a ranked list according to lens model. This is done by altering the effective distances to gain information on potential lensed counterparts and assessing the behavior of gravitational waves in various lens models. We will then determine the overall performance change in a final simulation campaign.

INTRODUCTION

The observation of gravitational lensing of gravitational waves has many relevant applications in the fields of cosmology, astrophysics and astronomy. These include the localisation of merging black holes, testing gravitational wave speed of propagation and polarization content, and the detection of intermediate-mass or primordial mass black holes[1]. Gravitational lensing of electromagnetic waves is an important phenomenon, yet we overlook immense amounts of information about the universe by ignoring the gravitational lensing of gravitational waves. Thus, the accuracy and impact of our analyses of celestial bodies, their interactions, and spacetime itself drastically improve when we consider the latter's effects. Additionally, while the distribution of dark matter is traditionally analyzed by its lensing effect of a background source's EM waves, observable matter accounts for only 5% of the universe [2]. With gravitational lensing of GWs, astronomers can chart the dark matter distribution of the universe without relying on the presence of background light sources, using the lensing effects from binary black hole sources instead. Gravitational wave strain from these events can be measured at greater distances than the images formed from most gravitationally lensed, light-producing sources, making it more optimal for long range observations. Because gravity is a universal law, meaning all objects with mass experience it, dark matter clusters act as the lens in these events. Gravitational lensing of gravitational waves also provides us with new ways of testing general relativity and allows us to study various relativistic systems[3].

While participating in the 2023 LIGO WAVE program, I will conduct research aimed at improving the detectors' search sensitivity in registering sub-threshold, strongly lensed events. To accomplish this, I will develop a toy lens model, run this lens model through various simulations to obtain the relative time delay and magnification distributions, incorporate this information into the TESLA search pipeline by modifying the likelihood portion of the gstLAL code, and run a simulation campaign to determine the performance of these changes.

In this proposal, I provide background information on LIGO, gravitational waves, gravitational lensing, and the various search pipelines used in analysis, specifically the gstLAL and TESLA methods. I then further explain the objectives of this project and describe the methodology in accomplishing this research, including analyses of the toy lens models and potential code modifications. Finally, I provide a tentative overview of my working schedule for the project's duration.

BACKGROUND

What is LIGO?

Short for Laser Interferometer Gravitational Wave Observatory, LIGO searches for gravitational wave signals coming from deep space, likewise making the smallest and most accurate measurements to date. Similar experiments began in the 1960s and, with the development and further improvement of interferometric detectors, LIGO's first detector was completed in the early 2000s. The (now updated) detectors are located in Hanford, Washington and Livingston, Louisiana, making them around 3000 kilometers in distance from each other, or 0.01 lightsecond. The latter measurement is relevant because gravitational waves propagate at the same speed as light, which is a concept I will cover more of later. The detector's large separation helps determine any local noise (i.e. environmental or instrumental) and also helps confirm gravitational wave events when registered on both with the appropriate time delay. They also serve in measuring wave polarizations and

source sky localization [3]. To establish further confidence in these readings, the LIGO Scientific Collaboration (LSC) joined teams with Italy's VIRGO project in 2007. The next year, the National Science Foundation provided funding for Advanced LIGO, which became fully functional in 2015[4].

On September 14, 2015, during the first official observatory run O1, both LIGO detectors simultaneously observed gravitational wave GW150914, making it the first direct detection of the phenomenon. This observation corroborated Einstein's General Theory of Relativity, which predicted the nonlinear electrodynamics of black holes. Analysis showed GW150914 was in fact the coalescence of a binary black hole, which also marked the first observation of such an event. The following is discussed in more detail later but, for clarity, the signal increased by 115 Hz in 0.2 s. A neutron star binary or neutron star-black hole binary would not produce the required chirp mass or orbital frequency for this to occur, thus it's most probable that it was caused by a BBH[3].

As of the second half of LIGO's third observing run (O3B), there's been a total of 90 observed events[5]. This includes the previously described GW150914[3] and GW170817, which was the gravitational wave emitted from a BNS merger. The latter is the largest registered GW signal to date, with a combined signal to noise ratio (SNR) of 32.4[6]. In comparison, GW150914 had a combined SNR of 24, although the VIRGO detector was not in operation at the time of the event[3]. Figure 1 shows the current number and type of CBC events detected by the LVK collaboration.

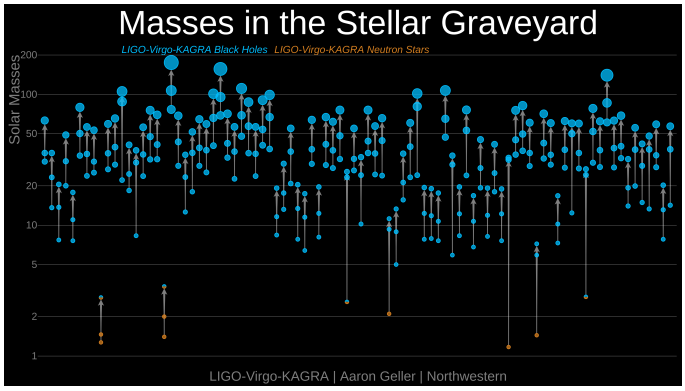

Figure 1. Masses in the Stellar Graveyard [Image credit: LIGO-Virgo/Aaron Geller/Northwestern]

Advanced LIGO operates using a modified Michelson interferometer, often called a Michelson-Morley interferometer. Each arm of the detector has a length of 4 km, meaning

$$L_x = L_y = L = 4\text{km}. \tag{1}$$

The large arm lengths are necessary because a typical gravitational wave produces displacements of only around 10^{-21}m. The detector's arms are placed in an L-shape because the compressions and expansions of spacetime caused by a GW are orthogonal, causing the arms to experience different amounts of displacement when a gravitational wave passes through. When this occurs, this difference in length is given by the equation

$$\Delta L(t) = \Delta L_x - \Delta L_y = h(t)L, \tag{2}$$

where h(t) is the gravitational wave strain[3]. However, instead of measuring displacements smaller than one-thousandth of a neutron, LIGO relies on the interference of light to detect such small changes. To detect this, a laser beam is directed towards a beam splitter such that half of the beam is reflected down one arm and the other half is transmitted down the other arm. Each end has a mirror to reflect the beam, and this reflected beam recombines at the photodetector, set to have destructive interference when there is no GW present. When a GW passes through, the length of the arms change such that the recombined light instead produces constructive interference. There is also a power-recycling mirror at the source that amplifies the power of the reflected wave from 20W to 100 kW, further helping the photodetector register the energy spike [3]. We measure this power output, which is really the phase difference between the recombined beams, and use transformation tools to derive the gravitational wave strain of the event.

What is a Gravitational Wave?

To understand gravitational waves, one must first realize the connection between space and time proposed by Einstein's General Theory of Relativity. Einstein began by exploring the relationship between gravitational mass, m_g, and inertial mass, m_i, which were simply assumed to be equal. Einstein did not make this assumption and instead worked on deriving the relationship from the bottom up. By studying the behavior of objects in a gravitational field, he realized that these two are equivalent only by accounting for the curvature of spacetime. This path is called a geodesic, and under this hypothesis, the equivalence of inertial and gravitational mass can be proven.

This led to the Equivalence Principle, which states that the only truly inertial state of an object in a gravitational field is in free-fall, or when it can move freely along its geodesic. This state of free-fall is called an inertial reference frame, or IRF. Instead of a force, Einstein proposed that gravity is a natural consequence of energy and mass interacting with spacetime, not each other. This is where the understanding of spacetime's fabric-like structure originates— the more massive an object is, the more it curves its specific region of spacetime. This ultimately led to the Einstein equation, which relates the geometry of spacetime to the distribution of matter and energy within it. The equation takes a 4×4 matrix, $T^{\mu\nu}$, describing the density and flow of matter and energy and outputs a 4×4 matrix (tensor), $G^{\mu\nu}$ describing the curvature of spacetime, given as

$$G^{\mu\nu} = 8\pi G T^{\mu\nu}, \tag{3}$$

where G is the gravitational constant. This equation shows the interdependence between matter and spacetime or, as John Wheeler famously said, that "spacetime tells matter how to move; matter tells spacetime how to curve." Specifically, $T^{\mu\nu}$ represents the Stress-Energy tensor defined as

$$T^{\mu\nu} = (\rho_0 + P_0)u^\nu u^\mu + P_0 g^{\mu\nu}, \tag{4}$$

where ρ_0 describes the object's density, P_0 describes its pressure and u^μ describes its four velocity, which is the object's motion in four-dimensional spacetime. The matrix given by $G_{\mu\nu}$ is also known as the Einstein tensor, which is constructed using the metric tensor and multiple contractions of the Riemann tensor, the only tensor capable of describing curvature. Thus, the Einstein tensor has the following equivalence:

$$G^{\mu\nu} \equiv R^{\mu\nu} - \frac{1}{2} g^{\mu\nu} R. \tag{5}$$

$R^{\mu\nu}$ is the Ricci tensor, R is the Ricci scalar and $g^{\mu\nu}$ is the metric tensor. The Ricci scalar is a contraction of the Ricci tensor, which is a contraction of the Riemann tensor. The curvature is described by $g_{\mu\nu}$, or the metric tensor describing the geometry of a particular region. For example, the weak field metric is defined as the Minkowski metric, $n_{\mu\nu}$, and a small perturbation term, $h_{\mu\nu}$, such that

$$g_{\mu\nu} = n_{\mu\nu} + h_{\mu\nu}. \tag{6}$$

Of course, the effects of a gravitational field cannot be completely dismissed for objects that aren't infinitesimally small. This is accounted for using tidal forces, which measures the stress/strain an object experiences while in a gravitational field. [7]

Because spacetime's geometry is dependent on the distribution of mass, accelerating objects will produce perturbations in spacetime that ripple outwards, known as gravitational waves. Anything with mass can produce gravitational waves, however most these waves are undetectable due to the larges distances traveled. Thus, we rely on extremely massive, rapidly accelerating objects for gravitational wave analysis, such as neutron stars and black holes. Objects like lone neutron stars (i.e. non-binary with a constant spin) produce continuous gravitational waves caused by irregularities in their shape and, as the name suggests, these gravitational waves have frequencies and amplitudes that change very slowly with time.

Nonetheless, there are many massive, extremely dense and rapidly moving bodies like neutron stars and black holes orbiting each other, known as binaries. Over time, these systems lose energy through gravitational radiation (i.e. by emitting gravitational waves), which causes their orbital distance to shrink and their acceleration to increase. This initial phase is known as the inspiral and has relatively stable readings by the detectors. Eventually, their orbital frequency gets large enough to noticeably affect the readings of their emitted gravitational wave, showing a gradual increase in amplitude and GW frequency. When these massive objects join, there's an extreme surge in energy and the gravitational wave strain peaks, called the merger stage. After merging, the joint bodies move to the ringdown stage. This three-step process is called compact binary coalescence, where compact describes extremely high-density objects. To better describe the specific system, these events are divided into three subclasses: binary neutron star (BNS), binary black hole (BBH), and neutron star-black hole binary (NSBH) mergers. Gravitational waves produced by these binary systems will be the focus candidates of the project. We can use the frequency f and its time derivative $\dot{f}$ obtained from the the Fourier transform of the strain amplitude to derive their source parameters, such as chirp mass M_c (measured in solar masses) where m_1 and m_2 are the masses of each object in the binary and

$$M_c = \frac{(m_1 m_2)^{3/5}}{(m_1 + m_2)^{1/5}} = \frac{c^3}{G}\left[\frac{5}{96}\pi^{-8/3} f^{-11/3}\dot{f}\right]^{3/5}. \tag{7}$$

In the case of GW150914, obtaining the chirp mass was essential in classifying the binary. Because $M \approx 30M_\odot$, this meant $m_{net} = m_1 + m_2 \geq 70M_\odot$. Only a binary black hole system could have the combined mass and orbital frequency capable of this, as a BNS wouldn't have the necessary mass while and NSBH system would have a much smaller orbital frequency. This event had an orbital frequency of 75 Hz, which is exactly half the gravitational wave frequency[3].

As mentioned, when gravitational waves propagate, they stretch and squeeze spacetime orthogonally. This results in two different types of polarizations: plus polarization, h_+, when the perturbations occur vertically/horizontally and cross polarization, $h_\times$, when they occur diagonally. We use this information in determining how the GW affects the geometry of spacetime and in deriving information about the source event's parameters. The two different polarizations are shown in figure 2.

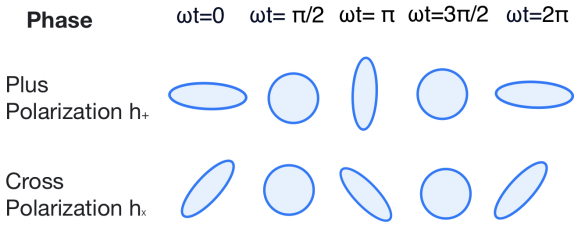

Figure 2. Diagram of h_+ and $h_\times$

It's worth noting that unresolved gravitational waves get collectively accounted for and termed stochastic background signal. This can only be statistically analyzed, as the collective behavior of microlensing events in a population of lenses contribute to this phenomenon. Furthermore, some of these gravitational waves likely originate from the Big Bang, making this a noteworthy field of study as it could help us better understand the primordial universe.

What is Gravitational Lensing?

Now that we've realized spacetime's non-Euclidean geometry, we can better understand the behavior of light in the presence of a gravitational field. Fermat's principle states that light always travels the path requiring the shortest amount of time, however that path is now a curve (called a geodesic) rather than a straight light. When light traveling through space encounters a gravitational field, it bends to follow the curvature of its geodesic. This effect is known as gravitational lensing and, while there are similarities to traditional lenses, this lens results from spacetime's interaction with a massive body rather than the wave's interaction with a medium. There are three classifications of lensing, which are described below.

Strong lensing occurs when the "lens" is extremely dense and massive and thus produces 2 or more images of the source, as in figure 3.

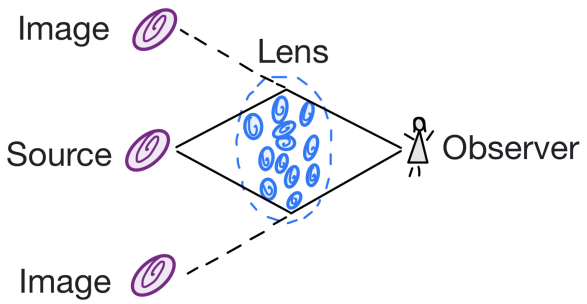

Figure 3. Strong lensing for a star forming galaxy

Weak lensing occurs when the lens object is massive and dense enough to deflect incoming light but doesn't have sufficient parameters to produce multiple images. Instead, the source image will appear distorted.

Microlensing accounts for the lensing effects of smaller celestial objects, such as stars. When stars pass in front of each other, light from the background source is temporarily brighter. However, this concept is not limited to interaction between stars. For example, microlensing helps us detect exoplanets by measuring the lensing star's change in brightness as an orbiting planet aligns with it and the observer.

While the study of gravitational lensing of light has been proven and widely studied, the possibility of gravitational waves undergoing gravitational lensing is still being explored. After analyzing data from the first half of LIGO/VIRGO's third observing run (O3a), the LVK collaboration (LIGO, VIRGO and KAGRA) concluded that there was no presence of strong lensing of GWs[8]. However, lensed counterparts are likely overlooked due to the effects of demagnification, time delay and morse phase differences. By assuming geometric optics, we're able to define the relative time delay, which represents the time difference between lensed signals coming from the same source. This also provides us with additional information about the morse phase factor. Under the same assumptions, we see that strong lensing can produce multiple events that differ only by their degree of magnification, or strain amplitude. Because we have yet to identify a pair of strongly lensed gravitational waves, we assume that the currently detected events are the magnified waveform, making their counterparts fall under the threshold due to demagnification effects. Other than a decrease in amplitude, these sub-threshold events have identical waveforms to their super-threshold counterparts. However, it's precisely this decreased amplitude that makes them undetectable with traditional analysis methods. We can describe gravitational waves (or the signal in the detector) using 15 different parameters, which are the masses m_1 and m_2, luminosity distance, inclination angle, coalescence phase, polarization, spin and the detector specific parameters of local coalescence time, local sky altitude, and local sky azimuth. A sub-threshold, strongly lensed GW will have the same parameters as the magnified waveform. This allows us to perform a more targeted search using information about the source, whose parameters are determined using Bayesian statistics.

What is a Lens Model?

The point-mass lens model is simplest way of analyzing gravitational lensing, which makes the assumption that the lens is simply a point mass. In this model, shown in figure 4, light travels along a straight line until it is bent by the lens and causes an image to appear at a deflection angle, $\hat{\alpha}$, from the source. This angle is calculated as follows

$$\hat{\alpha} = \frac{4G}{c^2}\frac{M}{\xi}, \tag{8}$$

where c is the speed of light $3 \times 10^8 \ \frac{m}{s}$, G is the gravitational constant $6.67 \times 10^{-11} \ \frac{Nm^2}{kg^2}$ and ξ is the impact parameter, which is the closest approach of light for a given lens. When c is set equal to unity, or c=1, we have

$$\hat{\alpha} = \frac{4GM}{\xi}. \tag{9}$$

By examining the equation, we see that $\hat{\alpha} \propto \frac{M}{\xi}$, meaning it depends only on the mass of the lensing system and the source's distance from the lens, measured orthogonal to the optical axis (the line connecting the observer to the lens). Thus, the lensing effect becomes more pronounced as the deflection angle increases[9].

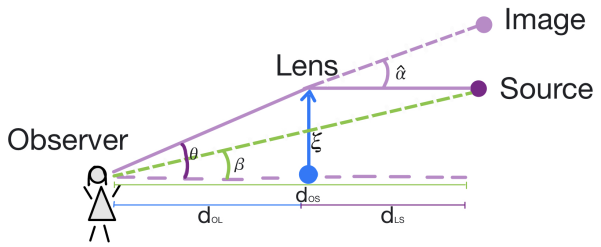

Figure 4. Point Mass Lens Model

If the source, lens and observer are perfectly aligned along the optical axis, infinitely many images form and are distorted into arcs that appear as a ring of light around the lens. The angular radius of an Einstein ring is given by the following equation:

$$\theta_E = \sqrt{4GM\frac{d_{LS}}{d_{OL}d_{OS}}}. \tag{10}$$

When we assume small angles, $\sin(\theta) \approx \theta$ and $\xi = \theta d_{OL}$. Furthermore, we see that the image is at height θd_{OS}, which is equivalent to $\beta d_{OS} + \hat{\alpha} d_{LS}$. Evaluating these values using the previous equations, we get

$$\theta d_{OS} = \beta d_{OS} + \hat{\alpha} d_{LS} \tag{11}$$

$$= \beta d_{OS} + d_{LS}\frac{4GM}{\xi} \tag{12}$$

$$= \beta d_{OS} + d_{LS}\frac{4GM}{\theta d_{OL}}, \tag{13}$$

and

$$\theta^2 = \theta\beta + 4GM\frac{d_{LS}}{d_{OS}d_{OL}} = \theta\beta + \theta_E^2. \tag{14}$$

Solving for θ using the quadratic equation,

$$\theta = \frac{\beta \pm \sqrt{\beta^2 + 4\theta_E^2}}{2}. \tag{15}$$

There are two solutions to this equation, meaning we see multiple images. Because $\sqrt{\beta^2 + 4\theta_E} > \beta$, multiple images form when $\beta \neq 0$, one at an angle θ_+ above the optical axis and another at an angle θ_- below it. When $\beta = 0$, this equation breaks down into the equation for an Einstein ring's angular radius, in which there are an infinite number of images. If we solve the lens equation for the time-delay, there are three different solutions depending on the type lensed signal, called Type I, II and III lensed signals. They represent the minimum, saddle-point and maximum solutions, respectively. Type II images are Hilbert transform of the unlensed waveform, while Type I and Type III images are scaled versions of it. Type III images differ from Type I only by their sign. In the case of LIGO, Type II images are prime candidates for detection given their similarity to the original waveform and consequential high SNR. This is because we assume geometric optics, in which waveform distortion only occurs when the image originates from a saddle-point solution[10].

However, the point-mass lens model fails in accounting for the mass distribution of the lensing galaxy. To approximate this better, we can instead employ the Singular Isothermal Sphere (SIS) model. It's best in modeling early-type galaxies, enabling us to approximate their surface density using the equation

$$\Sigma(x) = \frac{\sigma_v^2}{2G|\theta|} = \frac{\sigma_v^2}{2Gx\theta_E}. \tag{16}$$

Here, σ_v is the one-dimensional velocity dispersion of the lens[11].

Identifying Triggers

When searching for transient gravitational waves, we must account for the various sources of noise that contribute to our measurements. Thus, the output data from the detectors, $d(t)$, is a combination of both noise, $n(t)$, and gravitational wave signal, $h(t)$, such that

$$d(t) = n(t) + h(t). \tag{17}$$

There are various types of noise affecting our data, including environmental noise (earthquakes, human activity, etc.) and thermal noise (the non-zero temperature of the interferometer). Because noise is a random process, we make the assumption that it is Gaussian and stationary to better approximate the power output for a given bandwidth of signal. We obtain the energy of a time-function by integrating over the square of the function's magnitude, which we can relate back to the frequency space using Parseval's theorem. This shows

$$\int_{-\infty}^{\infty} |m(t)|^2 dt = \int_{-\infty}^{\infty} |\tilde{m}(f)|^2 df, \tag{18}$$

where the tilde over the function represents its Fourier transform and $P = m(t)$. This states that the total energy in the time domain is equivalent to the total energy in the frequency domain, meaning both of these expressions are proportional to the power at a given point. Furthermore, we see that the equation on the LHS is the traditional interpretation of energy in the time domain while the equation on the RHS measures energy in the frequency domain. Applying this concept to the noise within the data, we bound the integrals to reflect LIGO's observing time, T, and begin observing at time $t = T/2$ so we still have a two-sided domain. Letting $(-T/2, T/2)$ in the time domain correspond to $(-F, F)$ in the frequency domain, we see

$$\int_{-T/2}^{T/2} |n(t)|^2 dt = \int_{-F}^{F} |\tilde{n}(f)|^2 df. \tag{19}$$

Because the quantity inside the integral reflects energy per the respective variable of integration (i.e. J/s and J/Hz). If we further divide the inside quantity on the RHS by the

observing time, we obtain the average amount of energy produced by a given frequency during an observing run. Formally, this is called the double-sided power spectral density (PSD) of the noise, where

$$S^n_{double}(f) = \frac{|\tilde{n}(f)|^2}{T}. \tag{20}$$

Recall that this quantity originated from a double-sided integral covering both negative and positive frequencies. We are only concerned with measuring the positive frequencies, so we restrict the domain from 0 to F to obtain the single-singed PSD. Because we're only shifting the bounds, Parseval's theorem still holds, also implying that these integrals must be equal. Since the original function is even, by restricting the bounds to be positive, we halve the original value. Thus, to keep it unchanged we must double the value of the new integral. Pushing this constant multiple inside the function itself, then

$$S^n_{single}(f) = 2S^n_{double}(f) = \frac{2|\tilde{n}(f)|^2}{T}. \tag{21}$$

We can also define the PSD using the ensemble average $\langle|\tilde{n}(f)|^2\rangle$, which averages of all possible sets of waveforms creating noise at a given moment. This gives us an approximation of power output per bandwidth of signal, independent of time. To do this, we need to force the bandwidth to zero while still measuring non-zero power, so we must first normalize the data, sum the Fourier transforms of these infinitesimally small intervals, and finally take their average. If we plot this, we get a continuous curve representing the power distribution over all possible frequencies.

Nonetheless, this method isn't sufficient in measuring the PSD because $n(t) \neq 0$ as $t \to \pm\infty$, which is a condition of the Fourier transform. However, we work around this by considering the auto-correlation of the noise. This function reveals any patterns in the data by correlating the same noise function at two different times, t and $t + \tau$. As $\tau \to \pm\infty$, making the cross-correlated data approach 0 as required. We define the auto-correlated function of the noise as

$$R(\tau) = \langle n(t+\tau)n(t)\rangle = \int_{-\infty}^{\infty} n(t)n(t+\tau)dt. \tag{22}$$

Taking the Fourier transform of this, the single-sided noise PSD is now given by

$$S_n(f) = 2\int_{-\infty}^{\infty} R(\tau)e^{-i2f\pi\tau}d\tau. \tag{23}$$

Essentially, this function helps us approximate the power distribution while accounting for frequency variation. We use the auto-correlation function to determine the degree of correlation for a specific waveform within our time-series data (i.e. detecting repetitions and making the noise more predictable), then apply the Fourier transform to map this relationship into the frequency space. Also notice that when $\tau = 0$, the original time-series signal is squared, thus maximizing the auto-correlation function and the PSD. Additionally, because noise is real, we can say

$$\tilde{n}(-f) = \int_{-\infty}^{\infty} n(t)e^{-i2\pi(-f)t}dt \ = \tilde{n}^*(f), \tag{24}$$

where $\tilde{n}^*(f)$ represents the complex conjugate of the Fourier transform. Using this, we can further derive that

$$\langle\tilde{n}(f_1)\tilde{n}(f_2)\rangle = \frac{1}{2}S_n(f_1)\delta(f_1 - f_2), \tag{25}$$

where δ represents the Dirac delta function. When the noise is non-Gaussian, these equations no longer hold true. We call these glitches and, depending on their shape, they can be confused for potential gravitational waves.

Now that we've characterized noise, we can focus on searching for potential gravitational wave signal, $h(t)$, within the data. Because potential gravitational wave signals get buried underneath noise due to the incredibly small amplitude, we use various techniques of matched filtering. This allows us to measure the data using the signal-to-noise ratio (SNR), which is defined as

$$\rho = S/N, \tag{26}$$

where $S = \int \tilde{h}(f)\tilde{P}^*(f)df$ and $N^2 = [\langle\hat{s}^2\rangle - \langle\hat{s}\rangle^2]_{h(t)=0}$. N represents the root mean square value of the signal when there is no gravitational wave signal. $P(t)$ is the filter function, and $\tilde{P}^*(f)$ is the complex conjugate of its Fourier transform. We can maximize the SNR, ρ, by choosing $P(t)$ such that

$$\tilde{K}(f) = C\frac{\tilde{h}(f)}{S_n(f)}. \tag{27}$$

The overall SNR is also dependent on the number of detectors. This net value is given by

$$\rho^2_{net} = \sum_i \rho^2_i. \tag{28}$$

Because the strains of gravitational waveforms are inversely proportional to their effective distance D_{eff}, the optimal SNR is also inversely proportional to the effective distance. That is,

$$\rho_{opt} = \frac{1}{D_{eff}}. \tag{29}$$

Currently, detector sensitivity registers events with an $\rho > 4$.

One matched filtering pipeline used by LIGO is the gstLAL search pipeline, which essentially analyzes the data using filters pulled from a template bank and returns any potential matches as a trigger. After this, we use other methods to determine the statistical significance of the trigger, which gives the likelihood of it being an actual gravitational wave. Before we can run the data through the search pipeline, we must whiten it so the variance in amplitude is 1. If the amplitude of the data is higher than the variance (to a degree chosen by us), the pipeline disregards measurements in the $\pm$0.25s range, basically setting that interval's amplitude to 0. This process is

called gating, and it's important we choose this degree so we minimize noise error specifically from glitches while not overlooking any potential GWs. We then perform the single-value-decomposition (SVD) to reduce the waveform templates into a set of basic vectors. After this, we decompose the template bank so only the necessary waveforms are kept, which reduces the computational time. To do this, we use each template's parameters to determine their time-frequency evolution, then split the template bank into partially-overlapping split-banks according to this. We then clip any overlapping regions so only distinct waveform templates remain, and again whiten the data. We also divide the split-banks into time-slices and set each template to have the same number of sample points. This is because lower frequencies have more templates and are likewise susceptible to oversampling. Finally, SVD is again performed, now returning the most important basis waveform.

Next, the gstLAL maximizes the SNR by chopping the raw SNR time series data into 1s intervals. If the peak of a given interval passes above a certain threshold, it's marked as a trigger and the template parameters, trigger time, SNR and coalescence phase are recorded. These triggers then get sorted into a $\bar{\theta}$ bin. As mentioned, glitches can easily mimic gravitational waves and can thus be registered as triggers. We determine the statistical significance of the trigger using various methods, one being the consistency check (also called the chi-square test). With this, we can use the data from a single detector to compare the actual time series to the expected time series. We do this using the two out of phase yet identical matched-filter outputs such that

$$z_j(t) = x_{2j}(t) + ix_{2j+1}(t), \tag{30}$$

where $0 \leq j \leq N_T - 1$. We let $t = 0$ be the peak time t_p and compare this to the complex autocorrelation function

$$R_j(t) = \int \frac{|\tilde{h}_{2j}(f)|^2 + |\tilde{h}_{2j+1}(f)|^2}{S_n(|f|)} e^{2\pi i f t}. \tag{31}$$

At t_p, this is set to equal 0.5, which means $R_j(0) = 1$. We then determine the signal consistency text value χ^2 by normalizing the integral

$$\chi^2_j(t) = \frac{\int_{-\delta t}^{\delta t} |z_j(t) - z_j(0)R_j(t)|^2 dt}{\int_{-\delta t}^{\delta t} (2 - 2|R_j(t)|^2) dt}. \tag{32}$$

A stronger method of determining statistical significance is the coincidence criterion. Because there are multiple detectors with fixed locations, we can determine the time-frame in which the detectors should register the same gravitational wave signal. For example, because the LIGO Hanford and LIGO Livingston detectors are 0.01 light-seconds apart, their respective triggers for the same event should also occur within this general time-frame. However, because that time interval is specific to light, we increase the coincident time interval by a small amount to account for uncertainties in the GW's behavior. The gstLAL also enforces coincident triggers to have the same parameters, and together this information is used in determining the event's statistical significance. Now non-coincident triggers are marked as noise, which helps us better understand the probability density of each detector's noise background. From this, we determine the likelihood of the signal being a gravitational wave. The p-value represents the probability of noise producing the specific signal with an equal or larger ranking statistic, measured as $\ln \mathcal{L}$ for noise and $\ln \mathcal{L}^*$ for the specific trigger. Using these, we compute the False-Alarm Probability (FAP) such that

$$P(\ln \mathcal{L} \geq \ln \mathcal{L}^* | \text{noise}) = \int_{\ln \mathcal{L}^*}^{\infty} P(\ln \mathcal{L} | \text{noise}) d \ln \mathcal{L}. \tag{33}$$

We can also calculate the False-Alarm-Rate to determine the event's significance. This is similar to the FAP except it expresses how often the noise would produce a trigger with the necessary ranking statistic. We now have to consider the observing time T, and the total number of observed candidates, N, where

$$FAR = \frac{N \times FAP}{T}. \tag{34}$$

The gstLAL then ranks candidate events according to these ranking statistics. A smaller FAR means a lower likelihood of the candidate being produced by noise, thus increasing the likelihood of it being a real gravitational wave signal. Candidates are selected for further analysis if they go above a threshold decided by the analyst. This gives us a ranked list of possible candidates as well as the source parameters of the templates that identified them. However, source parameters can differ widely from the template parameters, so this list only serves in identifying candidates worthy of follow up analysis, not as a method of determining the actual source parameters. To do this, we obtain the posterior samples and derive the posterior probability distribution using Bayesian parameter estimation, which gives a better estimate of the source parameters[12].

The gstLAL search pipeline was established in 2008 and primarily contains elements of Python and C programming. Given LIGO's sensitivity to frequencies within the audible range, or approximately 10 Hz to 10 kHz, the gstLAL is based on an audio and video processing platform called Gstreamer. Gstreamer also operates as a pipeline, which allows us to sort and process large amounts of data. The gstLAL bases it's pipeline on this, including modifications necessary to analyze gravitational wave data.

Since it's origin, different packages of have been introduced depending on search type. If we are searching for compact binary coalescence events, we use the gstLAL-Inspiral package, which will be the package used for the duration of this project. There is also the gstLAL-Burst package for searching for gravitational wave bursts, the gstLAL-Calibration package for LIGO's strain data calibration, and the main gstLAL package which contains the core components for the various packages' codes. The gstLAL-ugly package is used for software development and, upon completion, code here gets transferred to its intended package.

The gstLAL-Inspiral was created with the intention of one day tracking real-time mergers producing electromagnetic radiation with telescopes. This is possible given the long inspiral phase of binary neutron star events, which corresponds to an increased time period of the signal observed by the detector. As the detector's sensitivity increases, the time frame between the initial trigger and the actual merger increases

When searching for CBC events, the gstLAL code operates using two different modes. The "low latency" mode searches real-time data for triggers from a binary merger, analyzing the data within a tenth of a second. The "offline" search prioritizes detail over return time, making use of more elegant code [13].

Searching for Lensed Pairs

Although this method is sufficient in detecting gravitational waves, it may fail in detecting sub-threshold lensed counterparts because they have low ranking statistics and are more easily buried in the noise background. However we can remedy this using the gstLAL-based TargetEd Sub-Threshold Lensing SeArch pipeline (TESLA). With TESLA, we take the known information about the super-threshold candidate and reduce the template bank so only templates with reasonable source parameters remain. Because the source parameter estimation of the super-threshold GW gives us a probability distribution rather than a fixed value, we also obtain the proper parameter estimation for the sub-threshold event using the Bayesian posterior probability distribution. This helps in reducing background noise while keeping the relevant template waveforms. If the noise is Gaussian and stationary, keeping only the space enclosed by the 90% credible region is sufficient in covering the sub-threshold counterparts. Yet most noise is non-Gaussian and a leading cause of false alarms, so this region is insufficient in searching for the targeted GW. Thus, research aims at decreasing the amount of templates picking up unwanted background noise while keeping the templates necessary in picking up the desired foreground information, i.e. the most probable template parameters.

This leaves us to decide what regions of the parameter space should be targeted, which is done by injecting samples of the sub-threshold signal and keeping only the templates that recover them using the gstLAL. To register as a trigger, it still requires an $\rho > 4$ so we tweak one of the original parameters. Because the source's effective distance D_{eff} is inversely proportional to the SNR, we can "demagnify" the confirmed waveform SNRs by increasing the measured effective distance. During an injection period, there is one injection with the original SNR and 9 weaker injections to describe the SNRs at the increased effective distances. The weaker injections are determined so the weakest injection registers an $\rho \geq 4$ in all detectors. We then inject the signals into our data and run them through the gstLAL with a full template bank, keeping templates capable of recovering the injections and adding them to the reduced template bank. The results are then analyzed so templates that significantly deviate from our original source parameter's posterior space are discarded. We then use this reduced template bank to search for potential sub-threshold lensed counterparts within all possible data. After this, we create a priority ranking list using the FAR ranking statistics from the confirmed gravitational wave. As with traditional analysis, this gives the likelihood of the signal being astrophysical, not of it being a lensed counterpart. Overall, the TESLA method maximizes the efficiency of the search by producing a nearly optimal template bank and reduces the noise background by accounting for glitches. This process is again described in figure 5 below [12].

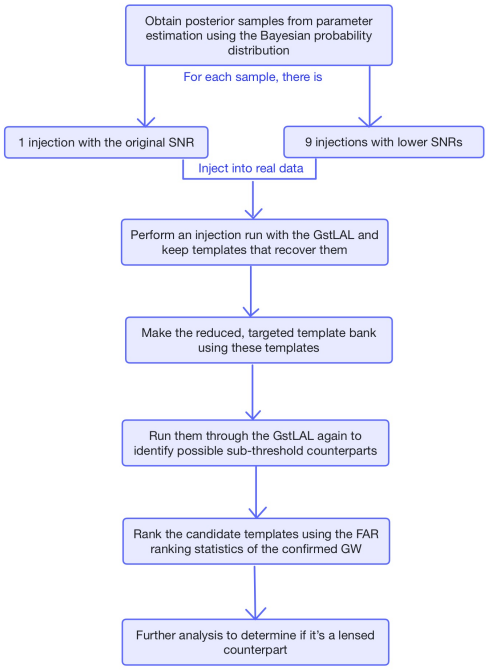

Figure 5. TESLA flowchart for a given target event

A test performed on the two LIGO detectors and the VIRGO detector using data from GW220112a showed that the TESLA template bank is the most effective in searching for sub-threshold counterparts. When compared to a single template bank containing the posterior samples from the target event with maximum probability, a PE template bank containing templates in the posterior probability distribution's 90% credible region and a template bank selected at random, the TESLA bank found $+9.26\%$ more injections than the general search. In comparison, the single, PE and random template bank missed more injections than the general search, having found percent changes of -40.0%, -80.3% and -77.5% respectively. Because the PE template bank only considers noise for the super-threshold event, it's more likely to miss the sub-

threshold event due to the time delay. The TESLA template bank takes into account the signal sub-space of the confirmed event and glitches, making it more likely to recover the lensed counterparts[12].

OBJECTIVES

The overall objective of this project is incorporating relative time delay and magnification distributions predicted by lens models into ranking possible sub-threshold, strongly-lensed candidates. Because the lens model calculations depend on multiple parameters of the lens system, such as lens mass and source distance, the search pipelines are most optimal when these various models are accounted for. This will provide us with ranking statistics based on the type of lens model used. The first step in this project is developing a toy lens model and running it through simulations to obtain the relative time delay and magnification values for varying parameter configurations. We then incorporate this information into the TESLA search pipeline by modifying the likelihood calculations in the gstLAL code. To determine the performance of these modifications, we will run a final simulation campaign. This method will improve the efficiency and effectiveness of the search if we see an increase in the number of astrophysical events registered by the detectors.

PROGRESS

In order to effectively run the gstLAL code, we first access LIGO's computer cluster using a Secure Server key. Through this, we submit the large-scale jobs needed to search for gravitational waves and monitor their progress. The gstLAL search pipeline offers various graphical interpretations of the signal within the detector, including closed and open box methods of charting the log likelihood of the noise and signal respectively. As mentioned, the log likelihood is defined as the ratio between the gravitational wave likelihood and noise likelihood, or

$$\ln \mathcal{L} = \frac{\mathrm{P}(\vec{O}, \vec{D_H}, \vec{\rho}, \vec{\mathcal{X}}_{eff}, [\Delta\vec{t}, \Delta\vec{\phi}]|\mathrm{signal})}{\mathrm{P}(\vec{O}, \vec{D_H}, \vec{\rho}, \vec{\mathcal{X}}_{eff}, [\Delta\vec{t}, \Delta\vec{\phi}]|\mathrm{noise})} \times \frac{\mathrm{P}(\vec{\theta}|\mathrm{signal})}{\mathrm{P}(\vec{\theta}|\mathrm{noise})} \tag{35}$$

$\vec{O}$ describes the participating detectors, $\vec{D}_H$ describes the horizon distances for each detector (or their maximum sensitivity), $\vec{\rho}$ describes the matched-filter SNR and $\vec{\mathcal{X}}_{eff}$ describes the auto-correlation based signal consistency test values. When the event in coincident, or occurs in multiple detectors, we also consider the time delay Δt and the phase delay $\Delta\vec{\phi}$ between the detections. The ratio of P($\vec{\theta}$|signal) and P($\vec{\theta}$|noise) represents how likely the template parameters are to model the trigger. As this value increases, the given template parameters are more likely to represent a signal than noise. [12] These individual probabilities are determined using Bayes theorem, where

$$\mathrm{P(hypothesis—data)} = \frac{\mathcal{L}(\mathrm{data}|\mathrm{hypothesis})\mathrm{P(hypothesis)}}{\mathrm{E(data)}}. \tag{36}$$

The final result is called the posterior, which is the probability used in the ratio for the log likelihood. We simply adjust the hypothesis to match whether we believe the data is signal or noise. $\mathcal{L}$(data—hypothesis) is the likelihood of seeing the data given the hypothesis, P(hypothesis) is the prior, or our initial belief, and E(data) is the evidence about our model. Unless working on model selection, the evidence is used only as a normalization constant such that

$$\mathrm{E(data)} = \int_{-\infty}^{\infty} \mathcal{L}(\mathrm{data—hypothesis})\mathrm{P(hypothesis)}. \tag{37}$$

This means the area under the curve of the probability distribution function always equals 1. Adding additional parameters to the hypothesis simply increases the number of products within the posterior calculation.

In analysis, we use the closed box method the compare the log likelihoods of the expected noise to the observed noise. If there is a trigger, the signal is first subtracted from this noise background so we may observe the noise behavior independently. We then compare the log likelihood of the full signal (including both noise and trigger) to the expected noise curve in the open box summary page, wherein we see the deviation of a potential GW signal. For example, while searching data for a trigger during O1, the closed-box summary is shown in the figure below.

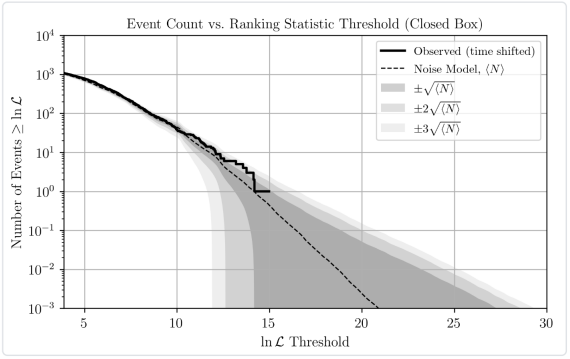

Figure 6. Event Count vs. Ranking Statistic Threshold for O1 (Closed Box)

We see that the observed noise follows the expected noise curve, within a small degree error. Looking at the open-box plot containing the noise and trigger below, we see that a single event deviates significantly from this.

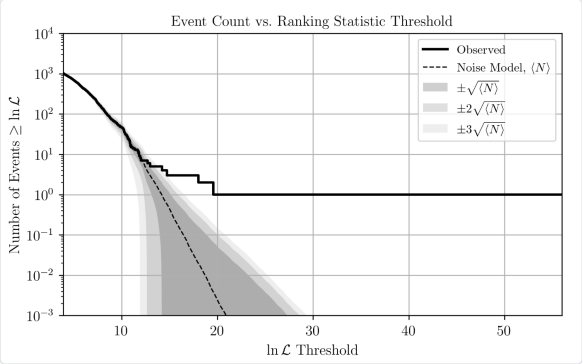

Figure 7. Event Count vs. Ranking Statistic Threshold for O1 (Open Box)

This event is in fact GW150914. Understanding the noise behavior alone helps confirm the veracity of this trigger, showing that signal detectable outside of the event follows our expectations [14]. Our goal is lowering this noise curve during the targeted search for lensed pairs so the subthreshold counterpart may be identified.

In modifying the likelihood portion of the code, we compare the probabilities of the signal being lensed versus unlensed rather than being a signal versus noise. Thus, the new log likelihood is defined to be

$$\ln(\mathcal{L}) = \frac{\mathrm{P}(t, \mu|\text{lensed})}{\mathrm{P}(t, \mu|\text{not lensed})} \times \frac{\mathrm{P}(\vec{\theta}|\text{lensed})}{\mathrm{P}(\vec{\theta}|\text{not lensed})}. \tag{38}$$

Here, t represents the time delay of the potentially lensed counterpart, or the time between its occurrence and the initial detection of the super-threshold event. Similarly, μ represents the magnification effects that occur because of the path difference.

WORKING SCHEDULE

1. Week 1: June 21 - June 23
   (a) Prepare computer with relevant software.
2. Week 2: June 26-June 30
   (a) Become familiar with the gstLAL search pipeline.
3. Week 3: July 3 - July 7
   (a) Learn how to access LIGO's computer cluster.
   (b) Run general searches in the gstLAL.
   (c) Prepare interim report 1.
4. Week 4: July 10 - July 14
   (a) Visit detector site.
   (b) Submit interim report 1.
   (c) Become familiar with portions of code set to be modified.
5. Week 5: July 17 - July 21
   (a) Modify likelihood calculations in gstLAL.
6. Week 6: July 24 - July 28
   (a) Continue modifying gstLAL code.
   (b) Prepare interim report 2 and abstract.
7. Week 7: July 31 - August 4
   (a) Prepare toy model.
   (b) Submit interim report 2.
   (c) Submit abstract.
8. Week 8: August 7 - August 11
   (a) Run final simulation campaign.
9. Week 9: August 14 - August 18
   (a) Determine overall efficiency of the project.
   (b) Prepare final presentation.
10. Week 10: August 21 - August 25
    (a) Final Presentation
11. Week 10+: September 4
    (a) Deadline for submitting final report.

[a] haleyboswell@live.com

[1] O. A. H. L. V. E. K. C. V. D. B. A. Renske A. C. Wierda, Ewoud Wempe, (2021).
[2] CERN, "Dark matter," .
[3] B. et al., PHYSICAL REVIEW LETTERS **116**, 061102 (2016).
[4] R. W. Kip Thorne, "A brief history of ligo," .
[5] LSC, "O3b catalog," .
[6] B. et al., PHYSICAL REVIEW LETTERS **119**, 161101 (2017).
[7] T. A. Moore, *A General Relativity Workbook* (2012).
[8] L. S. Collaboration and V. Collaboration, arXiv (2021), arXiv:2105.06384.
[9] LibreTexts, ed., *Big Ideas in Cosmology*.
[10] A. K. L. Y. C. Yijun Wang, Rico K.L. Lo, arXiv (2021), arXiv:2101.08264v2.
[11] M. Grespan, M.; Biesiada, Universe (2023).
[12] S. S. C. C. E. L. T. G. F. L. A. J. W. Alvin K. Y. Li, Rico K. L. Lo, arXiv (2022), arXiv:1904.06020v6.
[13] C. C. B. C. J. D. E. C. B. E. H. F. P. G. C. H. S. H. R. H. R. M. D. M. C. M. S. M. D. M. H. O. A. P. S. P. I. d. R. S. S. L. S. D. S. R. T. L. T. D. T. T. T. K. U. A. V. L. W. M. W. Kipp Cannon, Sarah Caudill, ArXiv (2020).
[14] gstLAL developers, (2021).